Microbiology Papers in Press. Published July 15, 2014 as doi:10.1099/mic.0.078717-0

Characterization of uncultured giant rod-shaped magnetotactic *Gammaproteobacteria* from a fresh water pond in Kanazawa, Japan

Azuma Taoka,[1,2]† Junya Kondo,[3]† Zachery Oestreicher,[1] and Yoshihiro Fukumori [1,2]#

[1]School of Natural System, College of Science and Engineering, Kanazawa University, Kakuma-machi, Kanazawa, Japan

[2]Bio-AFM Frontier Research Center, College of Science and Engineering, Kanazawa University, Kakuma-machi, Kanazawa, Japan

[3]Department of Life Science, Graduate School of Natural Science and Technology, Kanazawa University, Kakuma-machi, Kanazawa, Japan

Running title: Characterization of giant rod-shaped MTB

Category: Environmental and Evolutionary Microbiology

Correspondence: Yoshihiro Fukumori, e-mail: fukumor@staff.kanazawa-u.ac.jp, telephone: +81-76-264-6231, fax: +81-76-264-6230

The number of words: (i) the summary: 167 words; (ii) the main text: 4090 words

The number of tables: 1

The number of figures: 6

Footnotes: The DDBJ accession number for the 16S rRNA gene sequence of AB897514, where a new sequence has been determined.

†A.T. and J.K. contributed equally to this work.

Abbreviations: EDX, electron dispersive spectroscopy; FISH, fluorescence in situ hybridization; HRTEM, high-resolution transmission electron microscopy;

MMP, magnetotactic multicellular prokaryotes; MTB, magnetotactic bacteria; OAI, oxic-anoxic interface; OTU, operational taxonomic unit; SEM, scanning electron microscope; STEM, scanning transmission electron microscope; TEM, transmission electron microscope

Summary

Magnetotactic bacteria (MTB) are widespread aquatic bacteria, and are a phylogenetically, physiologically, and morphologically heterogeneous group; but they all have the ability to orient and move along the geomagnetic field using intracellular magnetic organelles called magnetosomes. Isolation and cultivation of novel MTB are necessary for a comprehensive understanding of magnetosome formation and function in divergent MTB. In this study, we enriched a giant rod-shaped magnetotactic bacterium (GRS-1) from a fresh water pond in Kanazawa, Japan. GRS-1 is unusually large (~13 μm by ~8 μm). It swims in a helical trajectory toward the south pole of a bar magnet by means of a polar bundle of flagella. Another striking feature of GRS-1 is the presence of two distinct intracellular biomineralized structures; the first are large electron-dense granules composed of calcium and the second are long chains of magnetosomes that surround the large calcium granules. Phylogenetic analysis based on the 16S rRNA gene sequence revealed that they belong to the *Gammaproteobacteria* and represent a new genus of magnetotactic bacteria.

INTRODUCTION

Magnetotactic bacteria (MTB) are a phylogenetically, morphologically, and metabolically heterogeneous group of prokaryotes that synthesize regular-shaped, nano-sized, single-domain magnetic particles of either magnetite (Fe_3O_4) or greigite (Fe_3S_4) in unique prokaryotic organelles called magnetosomes (Bazylinski & Frankel, 2004; Blakemore, 1975; Faivre & Schüler, 2008; Komeili, 2012). These function as a cellular magnetic compass in magnetotaxis motility that is directed along the geomagnetic field or in an applied magnetic field. Other intracellular structures that have been found in MTB are inclusions composed of elements such as phosphorus (Lins & Farina, 1999), iron-phosphorus (Byrne *et al.*, 2010), sulfur (Keim *et al.*, 2005), calcium (Isambert *et al.*, 2007), or polyhydroxybutyrate (Gorby *et al.*, 1988). Because of their involvement with these various ions, MTB probably play a significant role in geochemical cycling (Simmons *et al.*, 2007).

MTB are globally distributed in aquatic systems where there is an oxygen gradient such as lacustrine sediments or stratified water columns (Lefèvre & Bazylinski, 2013, Lefèvre & Wu, 2013, Lin, *et al*., 2013) where they can represent up to 30% of the natural bacterial communities (Spring *et al.*, 1993). The model for magnetotaxis is built on the idea that magnetotactic bacteria use their magnetosomes to navigate the oxic/anoxic interface (OAI) to find the ideal oxygen concentration (Spring & Bazylinski, 2006). They are phylogenetically diverse with members across three phyla, the *Proteobacteria*, *Nitrospirae* and Candidate division OP3. Most MTB in the *Proteobacteria* phylum belong to the *Alpha-*, *Gamma-* and *Deltaproteobacteria* classes (Lefèvre & Bazylinski, 2013). However, there are just four strains reported within the *Gammaproteobacteria*, two cultured (Lefèvre *et al.*, 2012) and two uncultured (Wang *et al.*, 2013). Given that MTB can be found in many different types of aquatic

environments and their identification is restricted to the cells that can be isolated using the racetrack method (Wolfe *et al.,* 1987) suggests their diversity is underestimated. This is particularly true for the magnetotactic members of the *Gammaproteobacteria* which were only discovered in 2012.

In this study, we isolated and characterized the largest known single celled MTB. The organism's unusually large rod-shaped size, ~13 μm by ~8 μm, is not its only outstanding trait. It also contains more magnetosomes (hundreds per cell) than most other MTB, and also possesses unusually large calcium-rich granules that occupy most of the interior volume of the cell. The organism was isolated from a freshwater pond and was determined to be a member of the *Gammaprotebacteria* class. All of these traits distinguish it from the other two characterized *Gammaproteobacterial* MTB, which possess typical MTB characteristics, but were isolated from inland saline systems in the USA (BW-2 from Badwater Basin, Death Valley National Park and SS-5 from Salton Sea) (Lefèvre *et al.,* 2012). The uncommon features of our newly discovered magnetotactic bacteria pushes the boundaries of the limits of MTB diversity further out and precisely highlights the need to continue to pursue the identification of new MTB in the natural environment.

METHODS

Sampling and enrichment of GRS-1 cells. Samples of sediment (0-3 cm deep) and surface water were collected from near the edge of a shallow freshwater pond in Kanazawa, Japan (36°54′N, 136° 93 73′E) and placed into tightly capped 0.5 L glass bottles. Isolation was begun immediately on return to the laboratory. The MTB were magnetically concentrated by attaching the south pole of neodymium magnets (10 mm x 5 mm) to the outside of sample bottles just above the sediment/water interface. The bottles were kept in the dark for up to three hours to allows the magnetotactic cells to swim towards the magnet. A pipet was used to remove ~1.5 ml of sample from the inside of the bottle near the magnet and then placed into to a 1.5 ml plastic tube. To isolate large sized magnetotactic bacteria, we did not use the capillary racetrack method (Wolfe *et al*., 1987) that is commonly used to isolate MTB, because the large cell sized MTB could not pass through the cotton filter. Instead, a neodymium magnet was placed on one end of the 1.5 ml plastic tube and incubated for three hours and then a ~0.25 ml aliquot of fluid was collected near the magnet. This sample was observed using phase contrast microscopy on an Olympus CKX41 microscope (Tokyo, Japan). While viewing the sample in the microscope, individual GRS-1 cells were collected using a very fine tipped glass pipet. After collecting many GRS-1 cells, they were were further purified by centrifuging the collected cells at 2,000 ×g for 1 min, and then suspending the pellet in 150 µl of sterilized water. The centrifugation step was repeated a total of three times and the enriched GRS-1 cells were used for further analysis. All isolation steps were performed at room temperature.

Optical microscopy. The cell morphology was observed using phase contrast microscopy on a Nikon Eclipse Ti microscope (Tokyo, Japan), equipped with an iXon3

EMCCD camera (Andor Technology, Belfast, UK). A video of the cell motility was recorded using phase contrast microscopy on an Olympus CKX41 microscope (Tokyo, Japan), equipped with a Moticam 2000 digital camera (Shimadzu, Kyoto, Japan) using Motic Images Plus 2.1S software (Shimadzu, Kyoto, Japan). The swimming speed of GRS-1 was calculated by measuring the distance traveled between successive frames from the recorded movie (elapsed time between each frame = 0.1 sec). The motility of a cell was traced and colored using Adobe Photoshop software (Adobe, San Jose, USA).

Electron microscopy. To prepare the specimen for observation in the scanning electron microscope (SEM), the samples were fixed in 0.1 M phosphate buffer (pH 7.4) containing 2% glutaraldehyde, post-fixed with 0.1 M phosphate buffer (pH 7.4) containing 2% osmium tetroxide, dehydrated in a graded series of ethanol (30-100%), critical point dried and sputter coated with gold according to standard procedures. The cells were observed using a JSM-6320F SEM (JEOL, Tokyo, Japan) operating at 5 kV.

Whole cells specimens for observation in the transmission electron microscope (TEM) were prepared by placing a drop of cell suspension onto a formvar- and carbon-coated copper grid and then allowed to air dry. The grids were examined using a JEM 2000EX TEM (JEOL, Tokyo, Japan) operating at 120 kV. For preparation of ultrathin sections of GRS-1 cells, the samples were fixed in 0.1 M phosphate buffer (pH 7.4) containing 2% glutaraldehyde, post-fixed with 0.1 M phosphate buffer (pH 7.4) containing 2% osmium tetroxide, dehydrated in a graded series of ethanol (30-100%), and embedded in Quetol 812. Ultrathin sections 80-90 nm thick were obtained using an ultramicrotome (Leica Ultracut R, Nussloch, Germany), and mounted on 200-mesh formvar- and carbon-coated copper grids, stained with lead citrate and 2% uranyl acetate, and observed as described above. The elemental distribution within the cells was analyzed by EDX using a JEM-2010FEF (JEOL, Tokyo, Japan) operating at

200 kV equipped with a JED-2300 EDX detector (JEOL, Tokyo, Japan). High-resolution transmission electron microscopic (HRTEM) analysis of the crystals in the ultrathin sections was performed using a JEM-2010FEF (JEOL, Tokyo, Japan) operating at 200 kV.

Sequence analysis of the 16S rRNA gene. The genomic DNA of bacterial cells was extracted using Lyse and Go Reagent (Thermo Scientific, Waltham, USA). The 16S rRNA genes from the concentrated solution of large MTB were amplified by PCR using the universal primers 27f (5´-AGAGTTTGATCCTGGCTCAG-3´) and 1525r (5´-AAAGGAGGTGATCCAGCC-3´) (Lane, 1991). For amplification of the *Gammaproteobacterial* 16S rRNA genes, a *Gammaproteobacteria* specific primer gamma1 (5´-GTTCCCGAAGGCACR-3´, nucleotide positions 1024 to 1038 *Eschericha coli* 16S rRNA gene numbering) was used as the reverse primer. PCR products were cloned into a pMD20-T vector using the Mighty TA-cloning Reagent Set for PrimeSTAR (Takara Bio, Tokyo, Japan). DNA sequencing of the cloned PCR products were performed using the BigDye Terminator v3.1 Cycle Sequencing Kit (Applied Biosystems, Foster City, USA) and a capillary sequencer ABI PRISM 3100 Genetic Analyzer (Applied Biosystems, Tokyo, Japan). Sequence analysis was performed using the BLAST algorithm in GenBank (http://www.ncbi.nlm.nih.gov). 16S rRNA gene sequences, including isolated MTB, reference cultures, and environmental clones were aligned using the CLUSTAL W multiple alignment accessory application (Thompson *et al.*, 1994) in the BioEdit sequence alignment editor (Hall, 1999). A phylogenetic tree was constructed using the neighbor-joining method (Saitou & Nei, 1987) in MEGA software (v. 4.0) (Tamura *et al.*, 2007) using bootstrap values with 1000 replicates.

Fluorescence in situ hybridization (FISH). Based on the newly obtained 16S rRNA gene sequence of GRS-1, two oligonucleotide probes were designed, BIG-1 (5´-GCTCACCTCATAGCACG-3´; nucleotide positions 217 to 233, *Eschericha coli* 16S rRNA gene numbering), and negative probe CBIG (5´-CGTGCTATGAGGTGAGC-3´). Three types of controls were used, the bacterial universal probe EUB338 (5´-GCTGCCTCCCRTAGGAGT-3´; nucleotide positions 338 to 355), the *Betaproteobacteria* specific probe BET42a (5´-GCCTTCCCACTTCGTTT-3´, nucleotide positions 1027 to 1043; *E. coli* 23S rRNA gene numbering) (Manz *et al.*, 1992), and the *Gammaproteobacteria* specific probe GAM42a (5´-GCCTTCCCACATCGTTT-3´; nucleotide positions 1027 to 1043; *E. coli* 23S rRNA gene numbering) (Manz *et al*., 1992). The oligonucleotides BIG-1, BET42a, and GAM42a were labeled with Alexa561, while the oligonucleotide EUB338 was labeled with Alexa488. In the hybridization experiments, *Burkholderia oxyphila* NBRC 105797 (Otsuka *et al*., 2011) and *E. coli* cells were used as controls for *Beta*-, and *Gammaproteobacteria*, respectively. FISH was carried out according to protocols reported by Pernthaler *et al*. (2001). After hybridization, the samples were observed using a Nikon ECLIPSE Ti microscope (Nikon, Tokyo, Japan).

Nucleotide sequence accession number. The sequences of the 16S rRNA gene were deposited in the DNA Data Bank of Japan under accession number AB897514.

RESULTS AND DISCUSSION

Purification of giant rod-shaped magnetotactic bacteria

Most magnetotactic bacteria have been isolated from freshwater habitats and can be easily separated from sediment samples using a simple magnet and enriched using a capillary racetrack (Wolfe *et al*., 1987). In this study, most of the collected MTB were magnetotactic cocci (~1 μm in diameter), however we also observed unusually large rod-shaped MTB, which we named GRS-1 (Fig. 1(a) and Movie S1). These larger cells required an extra step of enrichment in order to separate them from the smaller MTB. GRS-1 cells were isolated and purified from smaller MTB using a customized glass capillary pipet and then centrifuged at low speed to further enrich the large rod-shaped cells (Fig. 1(b)). Even with these extra enrichment steps, other MTB still remained that could be seen using the light and electron microscopes.

Morphology and motility of GRS-1

There are many morphotypes of MTB including cocci, vibrio, spirilla, rods, and clusters of cells. Cells of GRS-1 are rod-shaped having a mean length of 12.9 ± 2.7 μm and width of 7.8 ± 1.0 μm (n = 100), and a maximum cell size of 20 μm long and 11 μm wide. These dimensions show that these cells are the largest single-celled magnetotactic bacteria reported to date. Recently, large rod-shaped MTB were isolated from a freshwater source in the Yellow Sea (Zhang *et al.*, 2013). These MTB were similar in length (mean length 10.07 ± 1.87 μm) to GRS-1, but they were much narrower (mean width of 3.51 ± 0.49 μm).

GRS-1 cells swim towards the south pole of a bar magnet in a helical trajectory at rates up to 32 μm/sec (n = 4) (Fig. 1(c) and Movie S2). This speed is slower compared to other MTB, which swim at speeds greater than 100 μm/sec

(Lefèvre *et al.*, 2010; Lin *et al.*, 2012). When viewed in the SEM, the oval shape of GRS-1 is discernable (Fig 2(a)), albeit a little distorted from the dehydration step during sample preparation. A bundle of flagella emerges from the base of one end of the cell. These appear to be twisted near the base of the cell, but then splay out farther away from the cell (Fig. 2(b) and (c)). The width of each flagellum filament was 56 nm (n = 13). These flagella were only visible in the SEM samples and not in the TEM samples. Perhaps this is because flagella are inadvertently removed during the sample preparation for TEM analysis.

Ultrastructures of the interior of the cell

TEM imaging reveals that the cells contain two distinct internal structures, long chains of crystalline structures and large electron-dense granules that occupy most internal space of the cells. The long chains of regularly spaced crystals, representing the magnetosomes, are clearly visible around the inside periphery of the cells, however they are often obscured by the large opaque granules (Fig. 3(a)). The cells contained at least 300 crystals, but the exact number could not be determined because they are hidden by the granules. The crystals' mean length was 54.6 ± 4.8 nm (n = 300) and had a mean shape factor (the short axis divided by the long axis) of 0.85 ± 0.06 (n = 300) (Fig. 3(b) and (c)) indicating it is a slightly elongated prism. The size of the crystals falls within the single domain size range (Butler & Banerjee, 1975), and the size and shape of the crystals indicate that they are similar to other magnetotactic bacteria (Pósfai *et al.*, 2013). The EDX analysis clearly indicates a large iron K alpha peak and a very small sulfur K alpha peak (Fig. S1(a)-(c)). Elemental maps of an ultrathin section of the cells demonstrate that iron and oxygen are concentrated where the crystalline structures exist (Fig. 4(a)-(d)). Although there does appear to be very minor amounts of sulfur, however we attribute this to originating from the background of the cell. The analysis of the

crystals using HRTEM unequivocally identified the magnetosome crystals as magnetite (Fig. 3(d) and (e)).

The other type of internal structures is large, electron-dense granules which occupy a large portion of the internal volume of the cell. The size of the granules ranges from 2.5 to 4.5 μm wide. We performed an EDX spot analysis on one of the granules in a cell, and found that it was composed mostly of calcium with very minor amount of carbon, sodium, oxygen, phosphorus, and silicon (Fig. S1 (d)-(f)). The copper peak was generated from the copper grid used to support the sample in the microscope. We then analyzed whole granules in a cell and made elemental maps of calcium and phosphorus, which demonstrated that they were composed predominately of calcium (Fig. 4(e)-(g)). However, a minor amount of phosphorus was detected but we assume that this was from the background of the cell. It is common for MTB to contain internal granules, especially phosphorous (Lins & Farina, 1999) and sulfur (Keim *et al.*, 2005), however calcium has been reported only once within MTB in the literature (Isambert *et al.*, 2007). But the role of calcium in GRS-1 cells remains undetermined.

There is no evidence to support the idea that GRS-1 is a multicellular magnetic prokaryote. The electron microscope images give no indication that GRS-1 is composed of multiple cells. For example, MMPs are typically comprised of dozens of individual cells, which can clearly be seen in cross-section in the TEM (Keim *et al.*, 2007a). In Figure 3(a) we show a whole cell, which does not demonstrate any indication of intracellular membranes or an interruption of the magnetosomes chains, which is true for the MMPs shown in the work of Keim *et al.*, (2007a). Moreover, Keim *et al.* (2007b) have shown SEM images of MMPs in which you clearly see a regular pattern of clusters of ovoid structures (the ovoid structures being individual cells). However, in our SEM image there is no indication of a regular pattern on the surface of GRS-1 (Fig. 2). Additionally, the swimming behavior of GRS-1 does not mimic the “ping-pong”

motility of all the known MMPs (Rodgers *et al*., 1990). Furthermore, our organism does not have peritrichous flagella characteristic of MMPs. GRS-1 was isolated from a freshwater environment, not a saline environment from which other MMPs were isolated. Finally GRS-1 swims much slower than MMPs, GRS-1 has a rate of 32 μm/sec while MMPs swim much faster, 90 μm/sec. Granted, these individual points do not in and of themselves exclude GRS-1 from being an MMP, but taken together they clearly show that GRS-1 is not an MMP.

Fluorescence in situ hybridization (FISH) and phylogenetic analysis

The phylogenetic and FISH analyses showed that GRS-1 belongs to the *Gammaproteobacteria* class. First, we analyzed 16S rRNA gene sequences that were amplified from the enriched GRS-1 sample by using Eubacterial-specific primers. The obtained 16S rRNA gene sequences had a large variation belonging to *Beta-*, *Gamma-*, and *Deltaproteobacteria* and *Firmicutes* (Table S1). Then, we performed FISH analyses using *Betaproteobacteria* and *Gammaproteobacteria* specific probes and found that the *Gammaproteobacteria* specific probe positively labeled the GRS-1 cells (Fig 5(a) and (b)), indicating that GRS-1 belongs to *Gammaproteobacteria*. We then amplified the 16S rRNA gene fragment from the enriched GRS-1 sample using the *Gammaproteobacterial* 16S rRNA gene specific primer. This resulted in thirty-three of the forty-two clones having identical 16S rRNA gene sequences (Table S2). Finally, we generated a FISH probe (BIG-1) using the specific sequence obtained from the 16S rRNA gene sequence to confirm that the obtained 16S rRNA gene sequence originated from GRS-1. The BIG-1 probe specifically recognized GRS-1 cells (Fig 5(c)), while the probe designed from the negative chain (CBIG-1), did not label the GRS-1 cells (Fig. 5(d)).

A phylogenetic tree based on the 16S rRNA gene sequence from the GRS-1

strain showed that this organism belongs to the *Gammaproteobacteria* class of the *Proteobacteria* phylum (Fig. 6). GRS-1 lies within the order *Thiotrichales*, which also contains the rod shape MTB BW-2 (Lefèvre *et al.*, 2012) as well as the uncultured MTB OTU 8 (Wang *et al.*, 2013) (Fig. 6). GRS-1 has 88%-90% sequence identity to the other four known MTB belonging to the *Gammaproteobacteria* and it is closest to the uncultured MTB OTU 8. This clone was also collected from a freshwater environment; however, no morphological information is known about this organism, so no morphological comparison can be made. The phylogenetic tree clearly indicates that GRS-1 is a phylogenetically different group than the previously known MTB in the *Gammaproteobacteria* (Lefèvre *et al.*, 2012; Wang *et al.*, 2013).

Only two of the four other MTB belonging to the *Gammaproteobacteria* have morphological information, SS-5 and BW-2. GRS-1 has phenotypic characteristics that are similar and different to SS-5 and BW-2. So far, all the MTB *Gammaproteobacteria* cells are motile, but have different types of flagella. BW-2 and GRS-1 both have a polar bundle of flagella, but SS-5 has a single polar flagella. All of the MTB *Gammaproteobacteria* contain magnetite crystals. SS-5 cells contain 20 ± 7 crystals/cell, have an octahedral habit, a shape factor of 0.74 ± 0.07, a mean length of 86 ± 27 nm, and width of 63 ± 19 nm. BW-2 cells produce 30 ± 9 magnetite crystals/cell; have an octahedral structure with a shape factor of 0.94 ± 0.04, a mean length of 67 ± 16 nm, and a mean width of 63 ± 15 nm. These are very similar to the size and shape of the crystals found in GRS-1, even though the environments were different (GRS-1 was from freshwater, SS-5 and BW-2 were from saline environments). The biggest difference between GRS-1 and the other *Gammaproteobacteria* are the presence of calcium granules, which GRS-1 had, whereas BW-2 contained phosphate inclusions and SS-5 contained phosphate and sulfur inclusions. Another big difference that distinguishes GRS-1 from the other known types of *Gammaproteobacteria* cells are the

size of the cells, GRS-1 cells have a mean much longer and wider than BW-2 and SS-5. Table 1 compares the characteristics of BW-2, SS-5, and GRS-1.

Conclusion

The first MTB belonging to the *Gammaproteobacteria* were identified and described in 2012, SS-5 and BW-2 (Lefèvre *et al.*, 2012). Since then, two other phylotypes have been identified, but not described (Wang *et al*., 2013). GRS-1 is the third MTB in the *Gammaproteobacteria* class to be described, and it has unique characteristics that set it apart from the other two (SS-5 and BW-2), such as the cell dimensions, number/size/organization of magnetosomes, velocity of motility, type of flagellum, type of intracellular inclusion, and habitat. The most noteworthy characteristics are the size of GRS-1, which is the largest of all the MTB, and the presence of intracellular calcium inclusions. Taken as a whole, these characteristics set this organism apart from all the other known MTB and raises the bar for the amount of diversity within MTB.

GRS-1 has the unique ability to sequester large amounts iron in the form of magnetosomes and large amounts of calcium in the form of intracellular inclusions. This ability makes this organism a unique model for the study of metal compartmentalization in unicellular organisms. In order to establish such models we first need to determine the genome of GRS-1 to understand the mechanisms of metal uptake and the synthesis of these metal-accumulating organelles. Once we understand this we could then investigate the use of GRS-1 in environmental applications such as bioaccumulation of metals like calcium, iron, and potentially other metals.

ACKNOWLEDGEMENTS

We would like to thank Dr. C. Watanabe (Kanazawa Univ.) for his helpful discussion about HRTEM. This work was supported by MEXT KAKENHI Grant Number

344 24117007 and JSPS KAKENHI Grant Number 25850051. This work was also
345 supported by the Institute for Fermentation, Osaka.

346

347 **REFERENCES**

348

349 **Butler, R. F. & Banerjee, S. K. (1975)**. Theoretical single-domain grain size
350 range in magnetite and titanomagnetite. *J Geophys Res* **80**, 4049-4058.

351

352 **Bazylinski, D. A. & Frankel, R. B. (2004).** Magnetosome formation in
353 prokaryotes. *Nat Rev Microbiol* **2**, 217-230.

354

355 **Blakemore, R. (1975).** Magnetotactic bacteria. *Science* **190**, 377-379.

356

357 **Byrne, M. E., Ball, D. A., Guerquin-Kern, J.-L., Rouiller, I., Wu, T.-D.,**
358 **Downing, K. H., Vali, H. & Komeili, A. (2010).** *Desulfovibrio magneticus* RS-1
359 contains an iron- and phosphorus-rich organelle distinct from its bullet-shaped
360 magnetosomes. *Proc Natl Acad Sci U.S.A.* **107**, 12263-12268.

361

362 **Faivre, D. & Schüler, D. (2008).** Magnetotactic bacteria and magnetosomes.
363 *Chem Rev* **108**, 4875-4898.

364

365 **Gorby, Y. A., Beveridge, T. J. & Blakemore, R. P. (1988).** Characterization of
366 the bacterial magnetosome membrane. *J Bacteriol* **170**, 834-841.

367

368 **Hall, T. A. (1999).** BioEdit: a user-friendly biological sequence alignment editor
369 and analysis program for Windows 95/98/NT. *Nucleic Acids Symp* **41**, 95-98.

370

371 **Isambert, A., Menguy, N., Larquet, E., Guyot, F. & Valet, J. P. (2007).**

Transmission electron microscopy study of magnetites in a freshwater population of magnetotactic bacteria. *American Mineralogist* **92**, 621-630.

Keim C. N., Solórzano, G., Farina, M. & Lins, U. (2005). Intracellular inclusions of uncultured magnetotactic bacteria. *Int Microbiol* **8,** 111-117.

Keim, C. N., Farina, M. & Lins, U. (2007). Magnetoglobus, magnetic aggregates in anaerobic environments. *Microbe* **2**, 437-445.

Keim, C. N., Martins, J. L., de Barros, H. L., Lins, U. & Farina, M. (2007). Structure, behavior, ecology and diversity of multicellular magnetotactic prokaryotes. In *Magnetoreception and magnetosomes in bacteria*, pp. 103-132. Edited by D. Schüler. Berlin, Heidelberg, Germany: Springer.

Komeili, A. (2012). Molecular mechanisms of compartmentalization and biomineralization in magnetotactic bacteria. *FEMS Microbiol Rev* **36**, 232-255.

Lane, D. J. (1991). 16S/23S rRNA sequencing. In *Nucleic acid techniques in bacterial systematics*, pp. 115–175. Edited by E. Stackebrandt & M. Goodfellow M. Chichester, United Kingdom: Wiley & Sons Press.

Lefèvre, C. T., Santini, C. L., Bernadac, A., Zhang, W. J., Li, Y. & Wu, L. F. (2010). Calcium ion-mediated assembly and function of glycosylated flagellar sheath of marine magnetotactic bacterium. *Mol Microbiol* **78**, 1304-1312.

Lefèvre, C. T., Viloria, N., Schmidt, M. L., Posfai, M., Frankel, R. B. &

Bazylinski, D. A. (2012). Novel magnetite-producing magnetotactic bacteria belonging to the *Gammaproteobacteria*. *The ISME Journal* **6**, 440-450.

Lefèvre, C. T. & Bazylinski, D. A. (2013). Ecology, diversity, and evolution of magnetotactic bacteria. *Microbiol Mol Biol Rev* **77**, 497-526.

Lefèvre, C. T. & Wu, L. F. (2013). Evolution of the bacterial organelle responsible for magnetotaxis. *Trends Microbiol* **21**, 534-543.

Lin, W., Li, J. & Pan, Y. (2012). Newly isolated but uncultivated magnetotactic bacterium of the phylum *Nitrospirae* from Beijing, China. *Appl Environ Microbiol* **78**, 668-675.

Lin, W., Bazylinski, D. A., Xiao, T., Wu, L. F. & Pan, Y. (2013). Life with compass: diversity and biogeography of magnetotactic bacteria. *Environ Microbiol* doi: 10.1111/1462-2920.

Lins, U. & Farina, M. (1999). Phosphorus-rich granules in uncultured magnetotactic bacteria. *FEMS Microbiol Lett* **172**, 23-28.

Manz, W., Amann, R., Ludwig, W., Wagner, M., & Schleifer, K. H. (1992). Phylogenetic oligodeoxynucleotide probes for the major subclasses of proteobacteria: problems and solutions. *Syst and Appl Microbiol **15***, 593-600.

Otsuka, Y., Muramatsu, Y., Nakagawa, Y., Matsuda, M., Nakamura, M. & Murata, H. (2011). *Burkholderia oxyphila* sp. nov., a bacterium isolated from

424 acidic forest soil that catabolizes (+)-catechin and its putative aromatic
425 derivatives. *Int J Syst Evol Microbiol* **61**, 249-254.
426
427 **Pósfai, M., Lefèvre, C. T., Trubitsyn, D., Bazylinski, D. A., & Frankel, R. B.**
428 **(2013).** Phylogenetic significance of composition and crystal morphology of
429 magnetosome minerals. *Front Microbiol* **4**.
430
431 **Pernthaler, A., Pernthaler, J. & Amann, R. (2002).** Fluorescence in situ
432 hybridization and catalyzed reporter deposition for the identification of marine
433 bacteria. *Appl Environ Microbiol* **68**, 3094-3101.
434
435 **Rodgers, F. G., Blakemore, R. P., Blakemore, N. A., Frankel, R. B.,**
436 **Bazylinski, D. A., Maratea, D. & Rodgers, C. (1990).** Intercellular structure in a
437 many-celled magnetotactic prokaryote. *Arch Microbiol*, **154**, 18-22.
438
439 **Saitou, N. & Nei, M. (1987).** The neighbor-joining method: a new method for
440 reconstructing phylogenetic trees. *Mol Biol Evol* **4**, 406-425.
441
442 **Simmons, S. L., Bazylinski, D. A. & Edwards, K. J. (2007).** Population
443 dynamics of marine magnetotactic bacteria in a meromictic salt pond described
444 with qPCR. *Environ Microbiol* **9**, 2162-2174.
445
446 **Spring, S., Amann, R., Ludwig, W., Schleifer, K. H., van Gemerden, H. &**
447 **Petersen, N. (1993).** Dominating role of an unusual magnetotactic bacterium in
448 the microaerobic zone of a freshwater sediment. *Appl Environ Microbiol* **59**,
449 2397-2403.

Spring, S., & Bazylinski, D. A. (2006). Magnetotactic bacteria. In *The Prokaryotes* (pp. 842-862). Edited by M. Dworkin, S. Falkow, E. Rosenberg, K.-H. Schleifer, & E. Stackebrandt, New York: Springer.

Tamura, K., Dudley, J., Nei, M. & Kumar, S. (2007). MEGA4: Molecular Evolutionary Genetics Analysis (MEGA) software version 4.0. *Mol Biol Evol* **24**, 1596-1599.

Thompson, J. D., Higgins, D. G. & Gibson, T. J. (1994). CLUSTAL W: improving the sensitivity of progressive multiple sequence alignment through sequence weighting, position-specific gap penalties and weight matrix choice. *Nucleic Acids Res* **22**, 4673-4680.

Wang, Y., Lin, W., Li, J. & Pan, Y. (2013). High diversity of magnetotactic *Deltaproteobacteria* in a freshwater niche. *Appl Environ Microbiol* **79**, 2813-2817.

Wolfe, R. S., Thauer, R. K, & Pfennig, N. A. (1987). A ‘‘capillary racetrack’’ method for isolation of magnetotactic bacteria. *FEMS Microbiol Ecol* **45**, 31–35.

Zhang, W. Y., Zhou, K., Pan, H. M., Yue, H. D., Jiang, Y., Xiao, T. & Wu, L.-F. (2013). Novel rod-shaped magnetotactic bacteria belonging to the class *Alphaproteobacteria*. *Appl Environ Microbiol* **79**, 3137-3140.

475 Table 1. Comparison of the characteristics of all known magnetotactic bacteria

476 belonging to the *Gammaproteobacteria* class*†§

Strain	Order	Shape	Cell size L x W (μm)	Inclusion(s)	Crystal type	Crystal shape	Crystal length (μm)
BW-2	Thiotrichales	Rod	4.4 x 2.2	Sulfur, phosphorus	Magnetite	Octahedral	67
SS-5	Chromatiales	Rod	2.5 x 1.2	Phosphorus	Magnetite	Octahedral (elongated)	86
GRS-1	Thiotrichales	Rod	**12.9 x 7.8**	**Calcium**	Magnetite	Octahedral (elongated)	**54**

Strain	Crystal number	Magnetosome chain	Habitat	Flagellum	Speed (μm/sec)	Reference
BW-2	30	Single	Brackish, sulfidic spring	Bundle, polar	92	Lefèvre *et al.*, 2012
SS-5	20	Single	Saline	Single, polar	49	Lefèvre *et al.*, 2012
GRS-1	**>300**	**Many**	**Fresh water**	Bundle, polar	**32**	This paper

477

478 *There is no data on the characteristics of OTU 7 or OTU 8 from Zhang *et al.* (2013).

479 †All the sizes listed are averages.

480 §Bold words in the GRS-1 row represent differences between GRS-1 and the other two *Gammaproteobacteria*.

481

482

Figure legends

Fig. 1. Morphology and motility of GRS-1. (a) Phase contrast microscopy images of north-seeking MTB at the edge of a drop that were magnetically collected from sediment. The double-headed arrow indicates a layer of smaller MTB (mainly cocci). The yellow arrowheads show examples of GRS-1 cells. (b) Purified GRS-1 cells that were separated from other magnetic cells. The white arrows in panels (a) and (b) indicate the direction of the magnetic field. (c) Tracing the motility of a GRS-1 cell by coloring sequential images. Scale bars: 10 μm in panel (a) & (b); and 5 μm in panel (c).

Fig. 2. SEM observation of GRS-1 cells. (a) Micrograph of a whole GRS-1 cell showing the bundle of flagella emanating from one end of the cell. The flagella are bundled immediately adjacent to the cell, but then splay out showing a large number of filaments. (b) Bundle of polar flagella with a twist in the bundle (arrow). (c) Magnified image from the rectangle box in panel (b) showing the area where the filaments begin to separate from one another. Scale bars: 2 μm in panel a; 1 μm in panel b; and 0.5 μm in panel (c).

Fig. 3. TEM observation of a GRS-1 cell. (a) Image of a whole GRS-1 cell illustrating several magnetosome chains near the periphery of the cell, and a large electron-dense granule occupying most of the volume within the cell. Inset: detail of one of the magnetosome chains showing their slightly elongated shape. (b) The size distribution and (c) shape factor of the crystals. The crystal size was determined as the mean value of the short axis plus the long axis. (d) High-resolution transmission electron microscopy image of a single crystal and

its (e) Fourier transform pattern. Scale bars: 5 μm in panel (a); 100 nm in the inset; and 2 nm in panel (d).

Fig. 4. Elemental distribution within GRS-1. (a) Brightfield STEM image of an ultrathin section of a GRS-1 cell containing a chain of opaque structures. (b-d) Elemental maps of iron (b), oxygen (c), and sulfur (d) of the same cell used for panel (a). Note that the elements of iron and oxygen strongly overlap with the opaque structures, indicating these are iron oxide crystals. Sulfur appears to be ubiquitous in the background of the cell. (e) Low magnification brightfield STEM image of a GRS-1 cell. Elemental map of calcium (f) and phosphorus (g) of the same image as panel (e). Scale bars: 1 μm in panels (a-d); and 2 μm in panels (e-g).

Fig. 5. Specific detection of GRS-1 by FISH analysis. (a-1 to d-1) Phase contrast microscopic images of enriched GRS-1 cells (white arrows) and cells added for hybridization controls, *E. coli* is the *Gammaproteobacterial* control (white arrowheads) and *Burkholderia oxyphila* is the *Betaproteobacterial* control (yellow arrowheads). (a-2 to d-2) Fluorescent microscope images following hybridization with Alexa568 labeled universal Eubacteria probe EUB338. (a-3 to d-3) Fluorescent images labeled with a specific bacterial probe; Alexa488 labeled *Gammaproteobacteria* specific probe GAM42a (a-3); Alexa488 labeled *Betaproteobacteria* specific probe BET42a (b-3); Alexa488 labeled BIG-1 designed in this study based on the 16S rRNA gene sequence obtained from the purified sample of large cells (c-3); and Alexa488 labeled the probe CBIG-1, the complementary oligonucleotide of the BIG-1 probe sequence (d-3). All scale bars: 10 μm.

Fig. 6. Phylogenetic tree based on 16S rRNA gene sequences, showing the position of strain GRS-1 in the *Gammaproteobacteria* class. Bootstrap values (higher than 50) at nodes are percentages based on 1000 replicates. The 16S rRNA gene sequence of *Chromobacterium violaceum*, a member of *Betaproteobacteria*, was used to root the tree. The accession number of the 16S rRNA gene sequences are given in parentheses. Bar represents 2% sequence divergence.

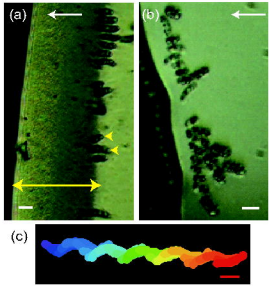
(a)
(b)
(c)

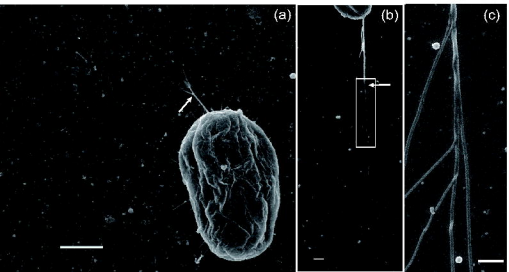
(a)
(b)
(c)

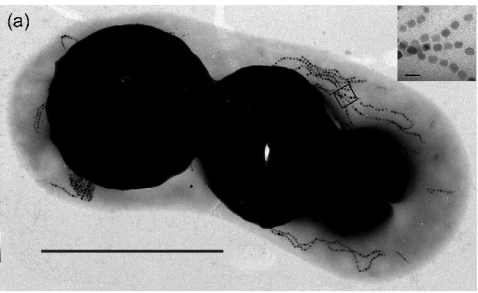
(a)

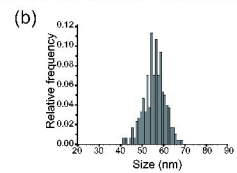
(b)
Relative frequency
0.12
0.10
0.08
0.06
0.04
0.02
0.00
20
30
40
50
60
70
80
90
Size (nm)

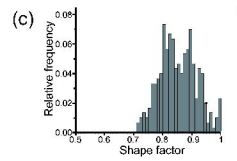
(c)
Relative frequency
0.08
0.06
0.04
0.02
0.00
0.5
0.6
0.7
0.8
0.9
1
Shape factor

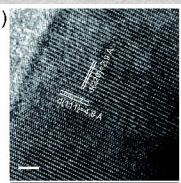
(d)
0.23 nm
0.19 nm
(111) d=2.3 Å

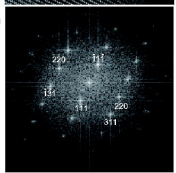
(e)
220
111
111
220
311

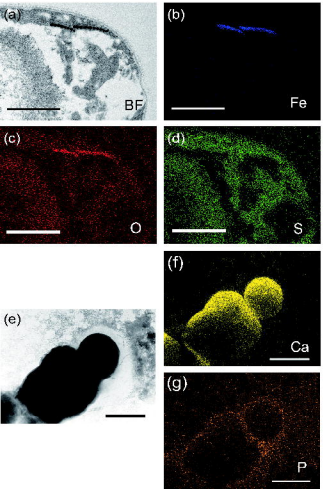
(a)
BF
(b)
Fe
(c)
O
(d)
S
(e)
(f)
Ca
(g)
P

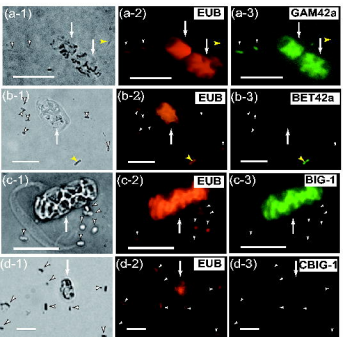
(a-1)
(a-2)
EUB
(a-3)
GAM42a
(b-1)
(b-2)
EUB
(b-3)
BET42a
(c-1)
(c-2)
EUB
(c-3)
BIG-1
(d-1)
(d-2)
EUB
(d-3)
CBIG-1

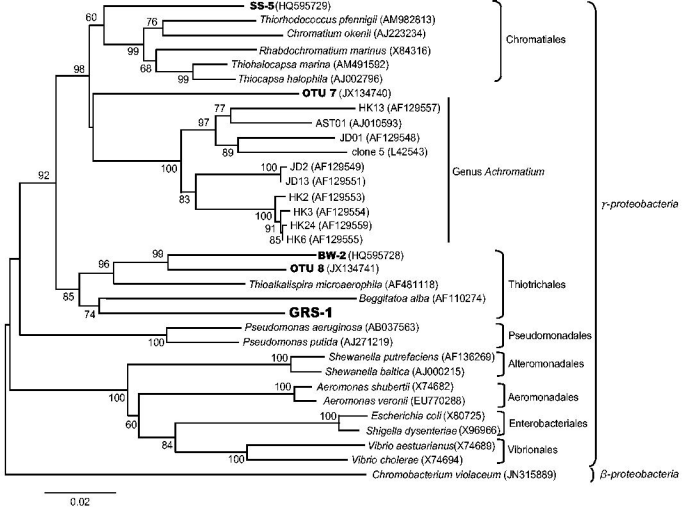
SS-5(HQ595729)
Thiorhodococcus pfennigii (AM982613)
Chromatium okenii (AJ223234)
Rhabdochromatium marinus (X84316)
Thiohalocapsa marina (AM491592)
Thiocapsa halophila (AJ002796)
Chromatiales
OTU 7 (JX134740)
HK13 (AF129557)
AST01 (AJ010593)
JD01 (AF129548)
clone 5 (L42543)
JD2 (AF129549)
JD13 (AF129551)
HK2 (AF129553)
HK3 (AF129554)
HK24 (AF129559)
HK6 (AF129555)
Genus Achromatium
γ-proteobacteria
BW-2 (HQ595728)
OTU 8 (JX134741)
Thioalkalispira microaerophila (AF481118)
Beggiatoa alba (AF110274)
GRS-1
Thiotrichales
Pseudomonas aeruginosa (AB037563)
Pseudomonas putida (AJ271219)
Pseudomonadales
Shewanella putrefaciens (AF136269)
Shewanella baltica (AJ000215)
Alteromonadales
Aeromonas shubertii (X74682)
Aeromonas veronii (EU770288)
Aeromonadales
Escherichia coli (X80725)
Shigella dysenteriae (X96986)
Enterobacteriales
Vibrio aestuarianus(X74688)
Vibrio cholerae (X74694)
Vibrionales
Chromobacterium violaceum (JN315889)
β-proteobacteria
0.02